

## Symbiotic contact process: Phase transitions, hysteresis cycles, and bistability

C. I. N. Sampaio Filho,<sup>1,\*</sup> T. B. dos Santos,<sup>1</sup> N. A. M. Araújo,<sup>1,2,3</sup> H. A. Carmona,<sup>1</sup> A. A. Moreira,<sup>1</sup> and J. S. Andrade Jr.<sup>1</sup>

<sup>1</sup>*Departamento de Física, Universidade Federal do Ceará, Fortaleza 60451-970, Ceará, Brasil*

<sup>2</sup>*Departamento de Física, Faculdade de Ciências, Universidade de Lisboa, Lisboa P-1749-016, Portugal*

<sup>3</sup>*Centro de Física Teórica e Computacional, Universidade de Lisboa, Lisboa P-1749-016, Portugal*



(Received 28 June 2018; published 6 December 2018)

We performed Monte Carlo simulations of the symbiotic contact process on different spatial dimensions ( $d$ ). On the complete and random graphs (infinite dimension), we observe hysteresis cycles and bistable regions, what is consistent with the discontinuous absorbing-state phase transition predicted by mean-field theory. By contrast, on a regular square lattice, we find no signs of bistability or hysteretic behavior. This result suggests that the transition in two dimensions is rather continuous. Based on our numerical observations, we conjecture that the nature of the transition changes at the upper critical dimension ( $d_c$ ), from continuous ( $d < d_c$ ) to discontinuous ( $d > d_c$ ).

DOI: [10.1103/PhysRevE.98.062108](https://doi.org/10.1103/PhysRevE.98.062108)

### I. INTRODUCTION

Improving our understanding of absorbing-state phase transitions in nonequilibrium systems is of great importance, not only because they occur in a variety of problems, but also display critical behavior and universality [1–3]. Absorbing states are those at which the dynamics is suppressed and no further changes occur. Examples of these states were found in models of epidemic spreading, opinion formation [4], population dynamics [5], diffusion-limited aggregation [6,7], traffic [8], and other nonequilibrium systems [9,10]. Most of these models are characterized by a continuous phase transition that falls into the directed percolation (DP) universality class [1,11,12]. However, absorbing phase transitions might also be discontinuous. Examples include the single-species restrictive contact process models, such as the quadratic contact process (QCP) [13–20], the Ziff-Gulari-Barshad (ZGB) model for catalysis [21–23], and ballistic deposition with anisotropic interactions [24,25].

The two-species contact process 2SCP was introduced by Oliveira *et al.* [26] to study the effects of symbiotic interactions in the contact process (CP) [27]. As in CP, in 2SCP the dynamics of each species evolves through sequences of creation and annihilation, but the rate of annihilation is reduced in the presence of a second species. Oliveira *et al.* have shown that, in the mean-field limit, the absorbing-state phase transition in 2SCP becomes discontinuous for a wide range of the symbiotic interaction strengths [26]. However, no evidence of a discontinuous transition in two dimensions has been observed from numerical simulations on a square lattice [26,28]. Here, we combine Monte Carlo simulations and a mean-field calculation to study the nature of the referred transition. We focus on the stability of the steady state and hysteretic behavior. In the mean-field limit, we confirm that the absorbing-state phase transition might be discontinuous,

while in two dimensions it is always continuous and belongs to the Directed percolation universality class [3,29].

The paper is organized as follows. In Sec. II we describe the 2SCP model and derive the phase diagram and bistable regions in the mean-field regime. The simulation results for different underlying networks are presented in Sec. III. In Sec. IV we draw some final conclusions.

### II. THE TWO-SPECIES CONTACT PROCESS

In the 2SCP two species ( $A$  and  $B$ ) are considered. Each site of a network is either empty or occupied by only one  $A$  particle, only one  $B$  particle, or two different particles. At a given instant  $t$ , the state of the site  $i$  is characterized by a pair of variables  $[\sigma_i(t), \eta_i(t)]$ , where  $\sigma_i(t) = 1$  ( $\eta_i(t) = 1$ ) if the site is occupied by one  $A$  particle ( $B$  particle) or  $\sigma_i(t) = 0$  ( $\eta_i(t) = 0$ ) otherwise. The generation of offsprings of a given type of particle occurs through catalytic creation processes. Precisely, the transition  $(0, \eta_i) \rightarrow (1, \eta_i)$  represents the creation of a particle  $A$  at site  $i$  and occurs at rate  $\lambda r_A$ , where  $r_A$  is the fraction of nearest neighbors (NN) occupied by  $A$  particles, independently of  $\eta_i$ . In the same way, the transition  $(\sigma_i, 0) \rightarrow (\sigma_i, 1)$  represents the creation of a particle  $B$  and occurs at rate  $\lambda r_B$ , with  $r_B$  being the fraction of NN occupied by  $B$  particles. Also, the offspring of a given particle can disappear at a site  $i$  through two annihilation processes, depending on the state of the site. For sites occupied just by one particle, the annihilation  $(1, 0) \rightarrow (0, 0)$  or  $(0, 1) \rightarrow (0, 0)$  occurs at unitary rate. However, the rate of annihilation is reduced on sites occupied by particles of both species (symbiosis), i.e., the annihilation  $(1, 1) \rightarrow (1, 0)$  or  $(1, 1) \rightarrow (0, 1)$  occurs at rate  $\mu \leq 1$ . Moreover, the density of particles is given by

$$\rho = \frac{1}{N} \sum_{j=1}^N (\sigma_j + \eta_j), \quad (1)$$

where  $N$  is the number of sites in the system.

\*cesar@fisica.ufc.br

In the 2SCP the symbiotic interaction favors the persistence of the doubled occupied sites, and the critical reproduction rate  $\lambda_c$  decreases as the parameter  $\mu$  is reduced. Moreover, a continuous phase transition in the Directed percolation universality class, is observed for  $\mu > 1/2$ . The upper critical dimension  $d_u$  of this model is the same of the ordinary CP, namely,  $d_u = 4$ . From the mean-field equations, it was previously found in Ref. [26] that the phase transition is discontinuous for  $\mu < 1/2$ , with  $\mu = 1/2$  identified as the tricritical point. In what follows, we study the stability of the steady state when the transition is discontinuous.

The state where  $(\sigma_i, \eta_i) = (0, 0)$  for all  $i$  is absorbing. At  $\lambda_c(\mu)$  the system undergoes an absorbing phase transition [26,28]. The mean-field theory for the 2SCP was first derived in Ref. [26], assuming spatial homogeneity. Defining  $p_0$ ,  $p_A$ ,  $p_B$ , and  $p_{AB}$  as probabilities for a given site to be empty, occupied by only one  $A$  particle, only one  $B$  particle, or by both species, respectively, they studied the effect of symbiotic interactions by seeking a symmetric solution  $p_A = p_B = p$ , which obeys

$$\frac{dp}{dt} = \lambda(1 - p_{AB} - 3p)(p + p_{AB}) + \mu p_{AB} - p, \quad (2)$$

and

$$\frac{dp_{AB}}{dt} = 2\lambda p(p + p_{AB}) - 2\mu p_{AB}, \quad (3)$$

using the constrain  $p_0 = 1 - 2p - p_{AB}$ . The absorbing state corresponds to  $p = 0$  and  $p_{AB} = 0$ . The active stationary solutions ( $dp/dt = 0$  and  $dp_{AB}/dt = 0$ ) are given by

$$p^\pm = \frac{\mu}{2\lambda(1 - \mu)} [2(1 - \mu) - \lambda \pm \sqrt{\lambda^2 - 4\mu(1 - \mu)}], \quad (4)$$

and

$$p_{AB}^\pm = \frac{\lambda(p^\pm)^2}{\mu - \lambda p^\pm}. \quad (5)$$

We define the order parameter as the density of particles  $\rho$ , which depends on both parameters  $(p^{0,\pm}, p_{AB}^{0,\pm})$ . Therefore, taking into account the steady-state solutions, we calculate  $\rho$  in the mean-field limit, for all values of the parameters  $\lambda$  and  $\mu$ . We focus on the limit  $\mu < 1/2$ , where the 2SCP undergoes a discontinuous phase transition [26]. Since only  $\rho \geq 0$  has physical meaning, there are three solutions, namely,

$$\rho_{\text{absorbing}} = 2p^0 + 2p_{AB}^0, \quad (6)$$

$$\rho_{\text{active}} = 2p^+ + 2p_{AB}^+, \quad (7)$$

and

$$\rho_{\text{unstable}} = 2p^- + 2p_{AB}^-, \quad (8)$$

where the indexes ‘‘absorbing,’’ ‘‘active,’’ and ‘‘unstable’’ refer to the type of solution, as discussed below.

One signature of a discontinuous transition is the presence of hysteretic behavior. Figure 1 shows the hysteresis cycle obtained from the mean-field calculation for the case  $\mu = 1/4$ . The solution  $\rho = 0$  (continuous red line) corresponds to the absorbing phase. The solutions  $\rho = 2p^+ + 2p_{AB}^+$  (dotted blue line) and  $\rho = 2p^- + 2p_{AB}^-$  (dashed green line) are physical if  $\lambda \geq \lambda_c(\mu)$  and  $\lambda_c(\mu) < \lambda < 1$ , respectively, with

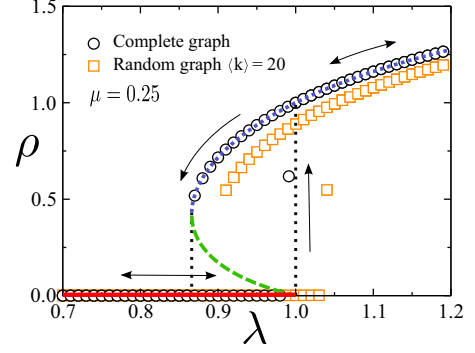


FIG. 1. Hysteretic cycle for  $\mu = 1/4$ , obtained from the mean-field calculation. Symbols represent simulations performed in complete graphs (circles) and random graphs (rectangles). The high-lighted arrows indicate the direction of the cycle. The solution  $\rho = 0$  (the red continuous line) corresponds to the stable absorbing state. The solution  $\rho = 2p^- + 2p_{AB}^-$  (the dashed green line) is unstable for any value of  $\lambda$ . Finally,  $\rho = 2p^+ + 2p_{AB}^+$  represents the stable active solution (the dotted blue line).

$\lambda_c = 2\sqrt{\mu(1 - \mu)}$ . Otherwise,  $\rho$  would admit complex values. For the case  $\mu = 1/4$ , we have  $\lambda_c = \sqrt{3}/4$ . However, as discussed next, the solution given by Eq. (8) is always unstable, while the stability of other solutions depends on the values of  $\lambda$  and  $\mu$ .

To analyze the stability of each solution, we consider the Jacobian matrix. The system described by Eqs. (2) and (3) can be written as  $\frac{dp}{dt} = f(p, p_{AB})$  and  $\frac{dp_{AB}}{dt} = g(p, p_{AB})$ . The Jacobian matrix is then

$$A(p, p_{AB}) = \begin{pmatrix} \frac{\partial f}{\partial p} & \frac{\partial f}{\partial p_{AB}} \\ \frac{\partial g}{\partial p} & \frac{\partial g}{\partial p_{AB}} \end{pmatrix}. \quad (9)$$

The trace  $\tau(\lambda, \mu)$  and the determinant  $\Delta(\lambda, \mu)$  of the matrix  $A$  for each steady-state solution are

$$\tau(p^0, p_{AB}^0) = \lambda - 1 - 2\mu, \quad (10)$$

$$\Delta(p^0, p_{AB}^0) = 2\mu(1 - \lambda), \quad (11)$$

$$\tau(p^\pm, p_{AB}^\pm) = 2\mu - \lambda - 1 \pm 2\sqrt{4\mu^2 - 4\mu + \lambda^2}, \quad (12)$$

and

$$\Delta(p^\pm, p_{AB}^\pm) = 4\mu^2 - 4\mu + \lambda^2 \pm (2\mu - \lambda)\sqrt{4\mu^2 - 4\mu + \lambda^2}. \quad (13)$$

This analysis can be summarized in Fig. 2, which shows the  $(\tau, \Delta)$  stability diagram of the Jacobian matrix for  $\mu = 1/4$  (the same parameters as in Fig. 1). The diagram is divided into five regions. Regions *I* and *II* correspond to the stable and unstable nodes, respectively. Regions *III* and *IV* correspond to the stable and unstable spirals. Finally, region *V* corresponds to the saddle points, namely, an unstable region. The solution  $\rho = 0$  (dashed red line) is conditionally stable, since for  $0 \leq \lambda \leq 1$ , this solution belongs to region *I* of stable nodes. However, for  $\lambda > 1$ , the absorbing solution is a saddle node (region *V*) and becomes unstable. The solution  $\rho = 2p^+ + 2p_{AB}^+$ , corresponding to an active phase, is stable

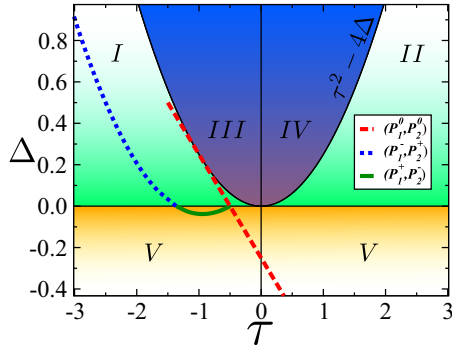


FIG. 2. The  $(\tau, \Delta)$  stability diagram of the mean-field solutions for  $\mu = 1/4$ . The regions *I*, *II*, *III*, *IV*, and *V* correspond to, respectively, the stable nodes, unstable nodes, stable spirals, unstable spirals, and saddle points. The solution  $\rho = 0$  (continuous red line) is stable if  $0 \leq \lambda \leq 1$ , since, from this condition, the absorbing solution lies in region *I*. For  $\lambda > 1$  the absorbing solution lies in region *V*, being therefore unstable. The active solution (dotted blue line)  $\rho = 2p^+ + 2p_{AB}^+$ , lies in the region *I* if  $\lambda \geq \lambda_c(\mu = 1/4) = \sqrt{3/4}$ . The solution  $\rho = 2p^- + 2p_{AB}^-$  (dashed green line) is unconditionally unstable, since for any value of  $\lambda$  this solution lies in region *V*.

if  $\lambda \geq \lambda_c = \sqrt{3/4}$ . Notice that in the range  $\sqrt{3/4} < \lambda < 1$  either absorbing or active phases are stable. This range, therefore, bounds the bistable region. Finally, the solution  $\rho = 2p^- + 2p_{AB}^-$  is unconditionally unstable, since for any value of  $\lambda$  this solution lies in region *V* of saddle nodes.

### III. COMPLETE AND RANDOM GRAPHS

In order to check the hysteretic behavior predicted by the mean-field calculation, we performed Monte Carlo simulations of the symbiotic contact process on complete and random graphs. A complete graph is defined as a structure where each node interacts with all others. The random graphs here considered are defined by the Erdős-Rnyi prescription [30] and constructed by the configuration model [31], where we first define the degree of each node and then connect them at random. In order to evolve the dynamics of 2SCP we considered the algorithm described in Ref. [26]. Accordingly, we define  $\delta t$  as the time increment associated with a given step in the 2SCP simulation and  $N_s$  and  $N_d$  as the number of sites occupied by one or two species, respectively. At each time step, we choose one of the following events:

- (1) Creation attempt at a site occupied only by a single species, with probability  $\lambda N_s \delta t$ .
- (2) Creation attempt at a site occupied by both species, with probability  $2\lambda N_d \delta t$ .
- (3) Annihilation of a particle at a site occupied only by a single species, with probability  $N_s \delta t$ .
- (4) Annihilation of a particle at a site occupied by both species, with probability  $2\mu N_d \delta t$ .

Since the probabilities are normalized,  $1/\delta t = \lambda N_p + N_s + 2\mu N_d$ , where  $N_p = N_s + 2N_d$  is the total number of particles. Moreover, we take  $\delta t = 1/N_p$  on the graphs of  $N_p$  active nodes, such that a Monte Carlo step corresponds to one attempt event per node, on average [32]. Using this algorithm, we follow the time evolution of the 2SCP. However, due to finite-size effects, the absorbing configuration can always

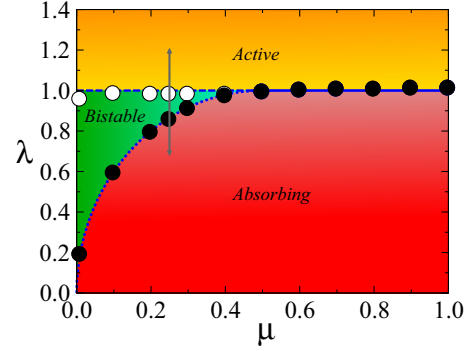


FIG. 3. The phase diagram of the symbiotic contact process. Three phases can be identified: Active, Bistable, and Absorbing. The continuous, dashed, and dotted lines represent solutions of the mean-field equations. For  $\mu > 1/2$ , the system undergoes a continuous phase transition between the active and absorbing phase. For  $\mu < 1/2$ , the system describes a discontinuous phase transition, defining a bistable region where the active and absorbing phases are both stable. The highlighted arrow indicates the direction of the transition for the case  $\mu = 0.25$ , where the bistable region is identified in the hysteretic cycle shown in Fig. 2. The open and solid symbols represent the critical reproduction rate  $\lambda_c$  obtained from simulations performed in complete graphs, with  $N = 5 \times 10^4$ . For the open symbols, the initial configuration is in the absorbing state, while for the solid symbols the fully occupied system defines the initial configuration.

be reached, even for  $\lambda > \lambda_c(\mu)$ , what would immediately suppress the dynamics [32,33]. To circumvent this problem, every time that an absorbing configuration is generated, we perform a spontaneous creation of two particles, one of each species, in sites chosen at random. Notice that this method guarantees that there will be at least one particle of each species at all times.

Figure 1 shows the density of particles for a complete graph (circles) and random graphs (rectangles) of  $N = 5 \times 10^4$  nodes. The hysteresis cycle was obtained for a fixed value of  $\mu = 1/4$ . For each value of  $\lambda$ , we allowed the dynamics to evolve for  $t_{\max}$  MCS. Next, we increased and decreased  $\lambda$  by constant intervals  $\Delta\lambda$ , and simulated the dynamics starting from the previous configuration, for each value of  $\lambda$  [34]. Each data point is an average over  $10^2$  independent configurations. As can be seen in Fig. 1, the results for the complete graph are in good agreement with the mean-field solutions. Moreover, both in the complete and random graphs the nature

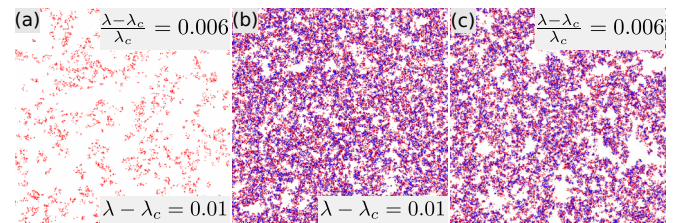


FIG. 4. Snapshots for ordinary and symbiotic contact processes. (a) Ordinary contact process at the distance 0.01 (absolute) or 0.006 (relative) from the critical point. (b) 2SCP at the same absolute distance of Fig. 4(a). (c) 2SCP at the same relative distance of Fig. 4(a).

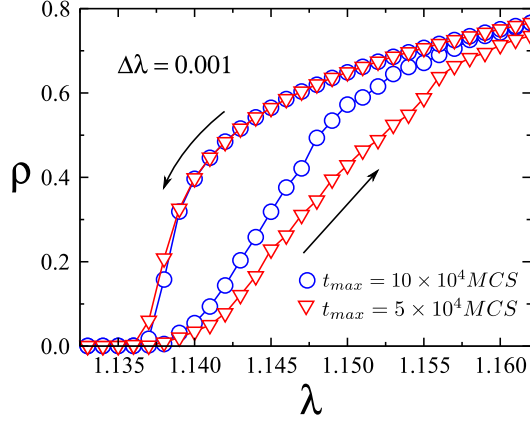


FIG. 5. Hysteresis cycles of the order parameter ( $\rho$ ) in terms of the creation rate  $\lambda$ , for  $\mu = 0.25$ , on a square lattice of linear size  $L = 200$ . Here we consider  $t_{\max} = 5 \times 10^4$  MCS (red triangles) and  $t_{\max} = 10 \times 10^4$  MCS (blue circles) as time increments. For each cycle, the control parameter  $\lambda$  is increased and decreased in the range  $1.0 \leq \lambda \leq 1.20$  at the constant intervals  $\Delta\lambda = 0.001$ .

of the hysteretic behavior is consistent with a discontinuous transition.

Figure 3 shows the phase diagram of the 2SCP obtained for a complete graph and mean-field solutions, where active, bistable, and absorbing phases are identified. For  $\mu > 1/2$ , the 2SCP undergoes a continuous absorbing-state phase transition. The solid symbols represent the critical parameter  $\lambda_c$  obtained by the ratio cumulant [2]. The continuous line represents the respective mean-field solution. For  $\mu < 1/2$ , the system undergoes a discontinuous phase transition with a bistable phase, where both the active and absorbing phases are stable. The initial configuration here is an absorbing state for the open symbols and a fully occupied state for the solid symbols. Notice the agreement between the simulated data (symbols) and the mean-field solutions.

#### IV. REGULAR SQUARE LATTICE

We now consider the 2SCP on regular square lattice. Figure 4 shows snapshots of the ordinary and symbiotic contact processes at the steady state for  $\epsilon = 0.001, 0.01, 0.05$ , where  $\epsilon = \lambda - \lambda_c$  and  $\lambda_c = 1.6488(1)$  [32] for the

ordinary contact process (Figs. 4(a)–4(c)) and  $\lambda_c(\mu = 0.25) = 1.13730(5)$  [26] for the 2SCP [Figs. 4(d)–4(f)]. For both models, the same method described for the complete and random graphs was used to avoid the absorbing state. Notice that, for any value of  $\epsilon$ , the density for active sites of the 2SCP is always greater than that for the ordinary contact process.

To determine the order of the phase transition on regular lattices, we analyze the hysteresis cycles. We employ the same algorithms used in Sec. III to produce the  $QS$  states and the hysteresis cycles. Figure 5 shows, for  $\mu = 0.25$ , the order parameter for two cycles in the creation rate  $\lambda$ . For each cycle, the control parameter  $\lambda$  is varied in the range  $1.0 \leq \lambda \leq 1.20$  at constant intervals  $\Delta\lambda = 0.001$ . Note that, as we double the value of  $t_{\max}$ , the width of the cycle is decreased. This indicates an absence of hysteretic behavior for  $t_{\max} \rightarrow \infty$ . Moreover, since the time necessary to reach the steady state diverges at the critical region in the thermodynamic limit, a system that undergoes a continuous phase transition to an absorbing phase should exhibit a hysteresis cycle when the control parameter is varied around its critical value [10,34].

The absence of bistability for the 2SCP on regular square lattices can be studied by evaluating the role of initial conditions on the stationary state, as described in Ref. [34]. Considering different values of the initial density  $\rho_0$  of particles, with fixed values of  $\lambda$  and  $\mu$ , we can evaluate the stability of each state. Figure 6 shows the results obtained on a regular square lattice, and on complete and random graphs. The values of  $\lambda$  and  $\mu$  are in a range where a possible bistable region is identified. As expected, for the complete and random graphs [Figs. 6(a) and 6(b)] the stable phase depends on the initial condition considered, reflecting the presence of a bistable region between the absorbing and active phases. However, on a square lattice [Fig. 6(c)] the active phase is always stable, for all considered initial conditions. This indicates that bistability is not observed for 2SCP on two-dimensional lattices. Moreover, we conjecture that the 2SCP always have a continuous phase transition below the upper critical dimension.

#### V. CONCLUSIONS

We have revisited the symbiotic contact process, where two species interact via a reduced death rate  $\mu$ , that describes

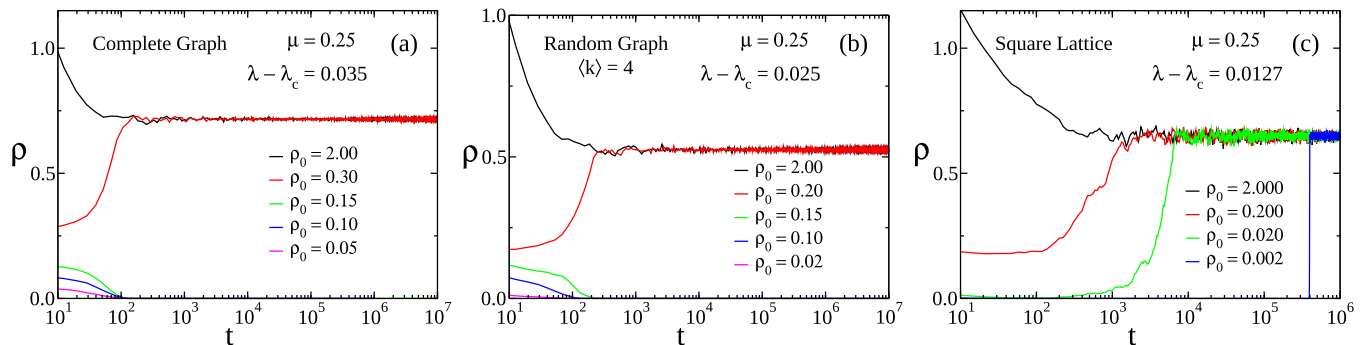


FIG. 6. The dependence of the initial density  $\rho_0$  of particles on stationary state. Accordingly, we have fixed the values of  $\lambda$  and  $\mu$  to identify a possible bistable behavior. (a) Complete graph,  $\mu = 0.25$  and  $\lambda - \lambda_c = 0.035$ . (b) Random graph,  $\mu = 0.25$  and  $\lambda - \lambda_c = 0.025$ . (c) Regular square lattice,  $\mu = 0.25$  and  $\lambda - \lambda_c = 0.0127$ .

the dynamics of doubled occupied sites, but individually, the dynamics of each species is described by an ordinary contact process. We have shown that, by using a suitable method to generate the quasistationary state (QS), the simulations performed on complete graphs are in accordance with the mean-field solutions. Precisely, these solutions reveal a discontinuous phase transition, with hysteretic behavior and a bistable phase, where the absorbing and the active phases are both stable. A bistable region also is detected on random graphs. Considering simulations on regular square lattices, we show the absence of hysteretic behavior and bistable regions, being those properties consistent with a continuous phase transition. Moreover, we conjecture that the 2SCP always undergoes

a continuous phase transition for any spatial dimension below the upper critical dimension, but above one-dimensional systems.

#### ACKNOWLEDGMENTS

We thank the Brazilian agencies CNPq, CAPES, FUNCAP, and the National Institute of Science and Technology for Complex Systems for financial support. N.A.M.A. acknowledges financial support from the Portuguese Foundation for Science and Technology (FCT) under Contract No. UID/FIS 00618/2013.

- 
- [1] G. Ódor, *Rev. Mod. Phys.* **76**, 663 (2004).  
 [2] R. Dickman and J. Marro, *Nonequilibrium Phase Transitions in Lattice Models* (Cambridge University Press, Cambridge, 2005).  
 [3] M. Henkel, H. Hinrichsen, and S. Lübeck, *Non-Equilibrium Phase Transitions*, Vol. 1 (Springer-Verlag, Berlin, 2009).  
 [4] C. Anteneodo and N. Crokidakis, *Phys. Rev. E* **95**, 042308 (2017).  
 [5] N. Sarkar, *Phys. Rev. E* **92**, 042110 (2015).  
 [6] M. J. Kartha and A. G. Banpurkar, *Phys. Rev. E* **94**, 062108 (2016).  
 [7] M. L. L. Iannini and R. Dickman, *Phys. Rev. E* **95**, 022106 (2017).  
 [8] N. V. Antonov, M. Hnatič, A. S. Kapustin, T. Lučivjanský, and L. Mižišin, *Phys. Rev. E* **93**, 012151 (2016).  
 [9] R. Gutiérrez, C. Simonelli, M. Archimi, F. Castellucci, E. Arimondo, D. Ciampini, M. Marcuzzi, I. Lesanovsky, and O. Morsch, *Phys. Rev. A* **96**, 041602(R) (2017).  
 [10] K. A. Takeuchi, M. Kuroda, H. Chaté, and M. Sano, *Phys. Rev. Lett.* **99**, 234503 (2007).  
 [11] P. Grassberger, *Z. Phys. B* **47**, 365 (1982).  
 [12] H. K. Janssen, *Z. Phys. B* **42**, 151 (1981).  
 [13] X. Guo, D.-J. Liu, and J. W. Evans, *Phys. Rev. E* **75**, 061129 (2007).  
 [14] D.-J. Liu, X. Guo, and J. W. Evans, *Phys. Rev. Lett.* **98**, 050601 (2007).  
 [15] X. Guo, D.-J. Liu, and J. W. Evans, *J. Chem. Phys.* **130**, 074106 (2009).  
 [16] F. E. da Silva and M. J. de Oliveira, *Comput. Phys. Commun.* **183**, 2001 (2012).  
 [17] C. Varghese and R. Durrett, *Phys. Rev. E* **87**, 062819 (2013).  
 [18] C. E. Fiore and G. T. Landi, *Phys. Rev. E* **90**, 032123 (2014).  
 [19] C. E. Fiore, *Phys. Rev. E* **89**, 022104 (2014).  
 [20] R. Pastor-Satorras, C. Castellano, P. Van Mieghem, and A. Vespignani, *Rev. Mod. Phys.* **87**, 925 (2015).  
 [21] R. M. Ziff, E. Gulari, and Y. Barshad, *Phys. Rev. Lett.* **56**, 2553 (1986).  
 [22] M. M. de Oliveira, M. G. E. da Luz, and C. E. Fiore, *Phys. Rev. E* **92**, 062126 (2015).  
 [23] M. M. de Oliveira, S. G. Alves, and S. C. Ferreira, *Phys. Rev. E* **93**, 012110 (2016).  
 [24] C. S. Dias, N. A. M. Araújo, and M. M. Telo da Gama, *Phys. Rev. E* **90**, 032302 (2014).  
 [25] N. A. M. Araújo, C. S. Dias, and M. M. Telo da Gama, *J. Phys.: Condens. Matter* **27**, 194123 (2015).  
 [26] M. M. de Oliveira, R. V. Dos Santos, and R. Dickman, *Phys. Rev. E* **86**, 011121 (2012).  
 [27] T. E. Harris, *Ann. Probab.* **2**, 969 (1974).  
 [28] M. M. de Oliveira and R. Dickman, *Phys. Rev. E* **90**, 032120 (2014).  
 [29] S. Lübeck, *Phys. Rev. Lett.* **90**, 210601 (2003).  
 [30] R. Albert and L. Barabási, *Rev. Mod. Phys.* **74**, 47 (2002).  
 [31] S. N. Dorogovtsev, A. V. Goltsev, and J. F. F. Mendes, *Rev. Mod. Phys.* **80**, 1275 (2008).  
 [32] R. Dickman, A. Vespignani, and S. Zapperi, *Phys. Rev. E* **57**, 5095 (1998).  
 [33] R. S. Sander, G. S. Costa, and S. C. Ferreira, *Phys. Rev. E* **94**, 042308 (2016).  
 [34] V. R. V. Assis and M. Copelli, *Phys. Rev. E* **80**, 061105 (2009).